Available online at www.sciencedirect.com
ScienceDirect
Trans. Nonferrous Met. Soc. China 25(2015) 520−526
Transactions of Nonferrous Metals Society of China
www.tnmsc.cn

Effect of Sn substitution for Co on microstructure and electrochemical performance of AB_5 type $La_{0.7}Mg_{0.3}Al_{0.3}Mn_{0.4}Co_{0.5-x}Sn_xNi_{3.8}$ (x=0−0.5) alloys

Julio Cesar Serafim CASINI[1,2], Zai-ping GUO[1], Hua Kun LIU[1],
Eliner Affonso FERREIRA[2], Rubens Nunes FARIA[2], Hidetoshi TAKIISHI[2]

1. Institute for Semiconducting and Electronic Materials, University of Wollongong, NSW 2522, Australia;
2. Materials Science and Technology Center, Nuclear and Energy Research Institute,
University of São Paulo, SP 05508-900, Brazil

Received 18 November 2013; accepted 11 March 2014

Abstract: The effects of substitution of Sn for Co on the microstructure, hydrogen storage and electrochemical discharge capacity of $La_{0.7}Mg_{0.3}Al_{0.3}Mn_{0.4}Co_{0.5-x}Sn_xNi_{3.8}$ (x=0, 0.1, 0.2, 0.3 and 0.5) alloys were investigated using X-ray diffraction (XRD), pressure composition isotherm (PCT) and electrochemical discharge cycle. XRD, scanning electron microscopy (SEM) and energy dispersive spectroscopy (EDS) tests showed that all of alloys are mainly composed of $LaNi_5$ and $MgNi_2$ phases, but when increasing the content of Sn in alloys, the LaNiSn phase appears and microstructure is refined. The PCT showed that increasing substitution of Sn for Co results in decrease of the maximum hydrogen storage capacity from 1.48% (x=0) to 0.85% (x=0.5). The electrochemical tests indicated that the maximum discharge capacity decreases from 337.1 mA·h/g (x=0) to 239.8 mA·h/g (x=0.5); however, the discharge capacity retention at the 100th cycle increases from 70.2% (x=0) to 78.0% (x=0.5).
Key words: hydrogen storage alloys; microstructure; Ni−MH batteries; Sn; Co; substitution

1 Introduction

Over the past years, $LaNi_5$-based hydrogen storage alloys for use in electrodes of rechargeable batteries have systematically incorporated specific alloying elements to improve the kinetics of hydrogen absorption and desorption, increase cycle life, improve corrosion resistance, etc. Cobalt, aluminium, manganese and magnesium are invariably present in the alloy composition [1].

What is known about Co is a very important element for improving the discharge capacity and prolonging the cycle lives of the electrodes alloys. For example, LIU et al [2,3] studied the effect of Co content on the structure, hydrogen storage and electrochemical performance of the $La_{0.7}Mg_{0.3}Ni_{3.4-x}Mn_{0.1}Co_x$ (x=0−1.6) alloys. Firstly, partial substitution of Ni by Co effectively improved the cyclic stability and the discharge capacity initially increased from 397.5 mA·h/g (x=0.00) to 403.1 mA·h/g (x=0.75) then a slight loss to 380.7 mA·h/g (x=1.60). Secondly, the appropriate substitution also increased the electrochemical kinetic performance of the alloy [2,3].

The typical commercial alloy, used as negative electrode of Ni−MH batteries, $MmNi_{3.55}Co_{0.75}Mn_{0.4}Al_{0.3}$, has high capacity and good cycling stability. It contains 10% of Co. However, Co takes up about 40% of the total cost of this alloy [4,5].

In the literature, there are several examples of Co-free and low-Co AB_5 type alloys. FERREIRA et al [6] investigated the influence of substitution of Co by Nb on $La_{0.7}Mg_{0.3}Al_{0.3}Mn_{0.4}X_{0.5}Ni_{3.8}$ (x=Co, Nb) alloys. Results showed that $NbNi_3$ phase appears on the microstructure and the discharge capacity decreases from 324 mA·h/g (Co) to 221 mA·h/g (Nb) [6].

Few investigations had been published based on substitution of Sn for Ni [7−10]. For example, KUMAR et al [10] reported a favourable charge−discharge cycling stability and good discharge capacity on the $LaNi_{4.25}Co_{0.5}Sn_{0.25}$ alloy. In this work, the microstructure, phase identification, hydrogen absorption isotherms, electrochemical capacity, cycling stability and high rate dischargeability of AB_5 type $La_{0.7}Mg_{0.3}Al_{0.3}Mn_{0.4}$-$Co_{0.5-x}Sn_xNi_{3.8}$ hydrogen storage alloys are investigated systematically.

Corresponding author: Julio Cesar Serafim CASINI; Tel: +55-11-31339248; Fax: +55-11-31339018; E-mail: jcasini@ipen.br
DOI: 10.1016/S1003-6326(15)63633-0

2 Experimental

The nominal composition of the studied alloys was designed as $La_{0.7}Mg_{0.3}Al_{0.3}Mn_{0.4}Co_{0.5-x}Sn_xNi_{3.8}$ (x=0, 0.1, 0.2, 0.3 and 0.5). The purities of all elements were at least 99.9%. The alloys were prepared by induction melting in a water-cooled copper crucible under the protection of argon atmosphere. The ingots were re-melted twice for homogeneity.

For X-ray diffraction (XRD), pressure composition isotherm (PCT) and electrochemical measurements, the alloys were mechanically pulverized and sieved through 200 mesh size (<75 μm).

Phase identification was performed on a GBC MMA X-ray diffractometer by Cu K_α radiation at 40 kV and 25 mA. The scan rate was 0.25 (°)/min with a step of 0.02° from 10° to 100°. The phase compositions were collected using Crystallographica-Search Match (CSM, PDF release 2002). The Rietveld refinement was obtained using Materials Studio 4.3.

In order to investigate the morphology and composition of the alloy, scanning electron microscopy (SEM) coupled with energy dispersive X-ray spectrometry (EDS) was used.

The PCT tests were conducted using a gas reaction controller, which is a product of Advanced Materials Corporation, USA. Before the measurement, each sample was put into a vessel and was evacuated at 30 °C for 1 h using a rotary vacuum pump, and activated 5 cycles. The PCT tests were performed at 30 °C until 3 MPa of hydrogen pressure. Hydrogen gas with purity above 99.99% was supplied from a cylinder.

All test electrodes were prepared by mixing alloy powder and nickel powder (<3 μm) with mass ratio of 1:4. The mixture was cold pressed under a pressure of 15 MPa (about 1 cm^2 in area and 0.1 mm in thickness). The discharge capacity of each electrode was measured in a flooded cell configuration using $Ni(OH)_2$/NiOOH as a counter electrode and 6 mol/L KOH solution as the electrolyte. The system was charged at 100 mA/g for 5 h followed by a 10 min rest and then discharged at 50 mA/g to the cut-off potential of 0.8 V. The high rate dischargeabilities were calculated after electrochemical cells were completely active.

3 Results and discussion

3.1 Microstructure and phase identification

The XRD patterns of the $La_{0.7}Mg_{0.3}Al_{0.3}Mn_{0.4}Co_{0.5-x}Sn_xNi_{3.8}$ (x=0−0.5) hydrogen storage alloys are shown in Fig. 1. It could be seen that the alloys are mainly composed of $LaNi_5$ ($CaCu_5$-type hexagonal structure) and $MgNi_2$ (hexagonal structure), while the $La_{0.7}Mg_{0.3}Al_{0.3}Mn_{0.4}Co_{0.5}Ni_{3.8}$ alloy shows (La,Mg)Ni_3 ($PuNi_3$-type rhombohedral structure) phase. The LaNiSn phase is formed and increased gradually when increasing x.

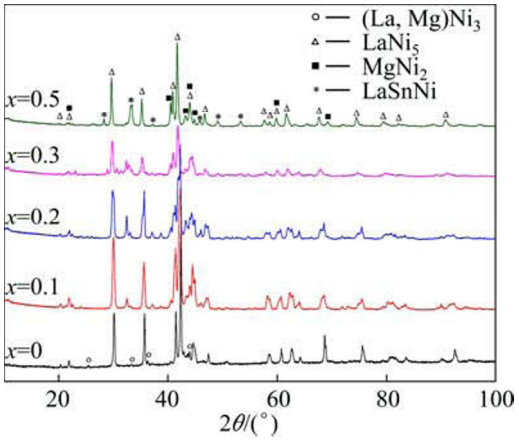

Fig. 1 XRD patterns of $La_{0.7}Mg_{0.3}Al_{0.3}Mn_{0.4}Co_{0.5-x}Sn_xNi_{3.8}$ (x=0−0.5) hydrogen storage alloys

The lattice parameters, unit cell volumes and the phase abundance of the alloys with different values of x obtained from Rietveld method of XRD analysis are listed in Table 1. It can be seen clearly that the parameters of a and c and the unit cell volumes of the $LaNi_5$ phase increase with increasing Sn content. Because the atomic radius of Co (1.35 Å) is smaller than that (1.45 Å) of Sn, the content of the $LaNi_5$ decreases from 75.44% (x=0) to 53.42% (x=0.5), while the content of LaNiSn increases from 4.44% (x=0.1) to 18.96% (x=0.5).

Figure 2 shows the SEM micrographs of the $La_{0.7}Mg_{0.3}Al_{0.3}Mn_{0.4}Co_{0.5-x}Sn_xNi_{3.8}$ (x=0−0.5) hydrogen storage alloys. Combining the results of XRD, SEM micrographs and EDS (Table 2) analysis shows that the $La_{0.7}Mg_{0.3}Al_{0.3}Mn_{0.4}Co_{0.5-x}Sn_xNi_{3.8}$ (x=0−0.5) alloys are composed of La- and Ni-rich phase ($LaNi_5$ phase, light grey regions), Mg- and Ni-rich phase ($MgNi_2$ phase, dark regions) and La-, Sn- and Ni-rich phase (LaNiSn phase, white regions) with small quantity of Mg content. As shown in Fig. 2(a), the composition of La, Mg and Ni ((La,Mg)Ni_3 phase, dark grey regions) is similar to the results reported by ZHANG et al [11] on the $La_{1.3}CaMg_{0.7}Ni_{9-x}(Al_{0.5}W_{0.5})_x$ alloys. When increasing the content of Sn, the content of LaNiSn phase increases gradually and more fine grains are found, which is similar for $LaNi_{4.0}Al_{0.2}Fe_{0.4}Cu_{0.4-x}Sn_x$ alloys studied by REN et al [12]. The further research would be to study the influence of annealing treatment on these alloys.

3.2 Pressure-composition-temperature (PCT) tests

PCT curves of the $La_{0.7}Mg_{0.3}Al_{0.3}Mn_{0.4}Co_{0.5-x}Sn_xNi_{3.8}$ (x=0−0.5) hydrogen storage alloys are

Table 1 Characteristics of alloy phase in $La_{0.7}Mg_{0.3}Al_{0.3}Mn_{0.4}Co_{0.5-x}Sn_xNi_{3.8}$ (x=0−0.5) hydrogen storage alloys

Sample	Phase	Space group (No.)	Parameter of fit R_{wp} /%	Phase content/%	Lattice parameter/Å			Cell volume/Å^3
					a	*b*	*c*	
	$LaNi_5$	*P*6/*mmm* (191)		75.44	5.029		4.051	88.73
x=0	$MgNi_2$	*P*63/*mmc* (194)	5.8	21.54	4.855		15.710	320.69
	$(La,Mg)Ni_3$	$R\bar{3}/m$ (166)		3.02	5.060		25.093	556.40
	$LaNi_5$	*P*6/*mmm* (191)		75.27	5.054		4.067	89.97
x=0.1	$MgNi_2$	*P*63/*mmc* (194)	12.5	20.29	4.843		15.297	310.72
	LaNiSn	*Pnma* (62)		4.44	7.563	4.613	7.571	264.14
	$LaNi_5$	*P*6/*mmm* (191)		72.98	5.064		4.082	90.65
x=0.2	$MgNi_2$	*P*63/*mmc* (194)	15.6	19.30	4.839		15.358	311.42
	LaNiSn	*Pnma* (62)		7.72	7.585	4.658	7.523	265.80
	$LaNi_5$	*P*6/*mmm* (191)		67.64	5.079		4.085	91.26
x=0.3	$MgNi_2$	*P*63/*mmc* (194)	13.6	18.48	4.816		15.598	313.309
	LaNiSn	*Pnma* (62)		13.87	7.629	4.729	7.406	267.19
	$LaNi_5$	*P*6/*mmm* (191)		65.44	5.088		4.107	92.08
x=0.5	$MgNi_2$	P63/*mmc* (194)	10.8	15.60	4.813		15.731	315.59
	LaNiSn	*Pnma* (62)		18.96	7.672	4.915	7.357	277.42

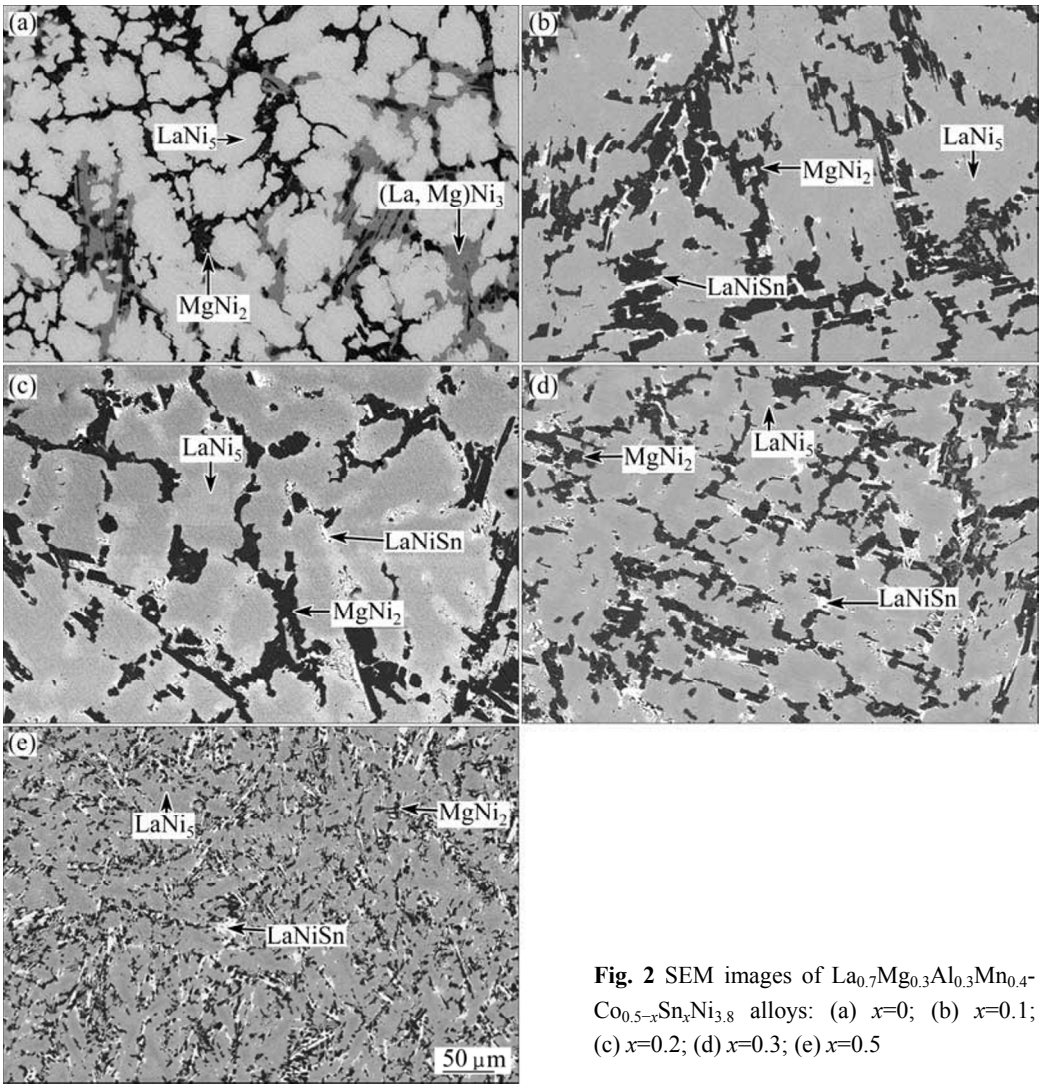

Fig. 2 SEM images of $La_{0.7}Mg_{0.3}Al_{0.3}Mn_{0.4}Co_{0.5-x}Sn_xNi_{3.8}$ alloys: (a) x=0; (b) x=0.1; (c) x=0.2; (d) x=0.3; (e) x=0.5

Table 2 EDS results for different phases identified in SEM images

Sample	Phase	Composition/%						
		La	Mg	Al	Mn	Co	Sn	Ni
	$LaNi_5$	15.4	<1	4.5	2.5	7.9	−	69.5
x=0	$MgNi_2$	<1	19.8	3.3	12.6	8.5	−	54.9
	$(La,Mg)Ni_3$	8.4	10.3	2.8	6.9	8.0	−	63.6
	$LaNi_5$	15.9	<1	4.8	3.5	6.8	1.2	67.3
x=0.1	$MgNi_2$	<1	21.9	3.8	10.5	7.3	<1	55.9
	LaNiSn	20.7	3.8	2.8	3.3	2.7	19.8	46.9
	$LaNi_5$	15.3	<1	4.9	3.2	4.9	3.2	67.9
x=0.2	$MgNi_2$	<1	21.2	3.3	10.7	6.5	<1	57.3
	LaNiSn	19.4	3.2	2.4	4.1	2.6	19.7	48.6
	$LaNi_5$	15.3	<1	5.2	3.9	2.9	5.3	66.7
x=0.3	$MgNi_2$	<1	21.3	3.4	11.5	2.9	<1	60.3
	LaNiSn	19.5	4.5	1.8	3.9	<1	19.6	49.9
	$LaNi_5$	15.7	<1	4.4	3.5	−	6.9	68.9
x=0.5	$MgNi_2$	<1	21.7	3.5	11.8	−	<1	61.5
	LaNiSn	19.8	4.1	2.3	3.2	−	20.4	50.2

shown in Fig. 3. It is seen that the maximum hydrogen storage capacity of the alloys decreases from 1.48% (x=0) to 0.85% (x=0.5), which could be attributed to the content of $LaNi_5$ reduced when Sn substituted Co. REN et al [12] reported that the substitution of Sn in $LaNi_{4.0}Al_{0.2}Fe_{0.4}Cu_{0.4-x}Sn_x$ alloys also decreased the hydrogen storage capacity.

These support that the optimized content of $LaNi_5$ phase and $(La,Mg)Ni_3$ phase improved the hydrogen storage capacity [13].

The PCT isotherm absorption−desorption hysteresis factor (H_f) was calculated by the following formula:

$$H_f = \ln\left(\frac{p_a}{p_d}\right) \quad (1)$$

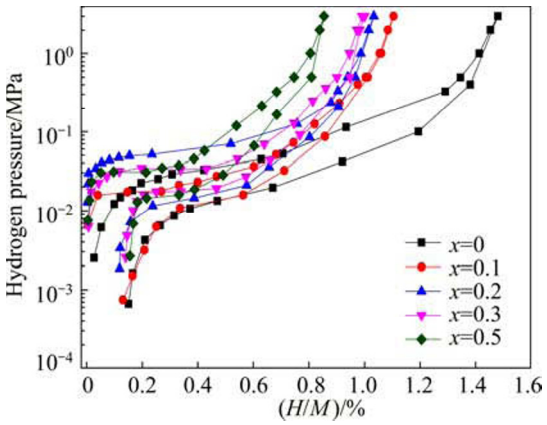

Fig. 3 PCT curves of $La_{0.7}Mg_{0.3}Al_{0.3}Mn_{0.4}Co_{0.5-x}Sn_xNi_{3.8}$ (x=0−0.5) alloys at 30 °C (H/M represents the hydrogen storage in a metal alloy)

where p_a and p_d are the absorption and desorption equilibrium pressures at 50% of hydrogen storage capacity. In Table 3, the slope factor (S_f) is the ratio of capacities between the middle region (defined between 0.01 and 0.5 MPa) and the entire reversible region. The data of H_f and S_f for each alloy are listed in Table 3.

Table 3 Maximum hydrogen storage capacity, H_f, and S_f of $La_{0.7}Mg_{0.3}Al_{0.3}Mn_{0.4}Co_{0.5-x}Sn_xNi_{3.8}$ (x=0−0.5) alloys

Sample	$(H/M)_{max}$/%	H_f	S_f/%
x=0	1.48	1.06	38.85
x=0.1	1.11	0.89	49.54
x=0.2	1.03	0.82	52.35
x=0.3	0.99	0.73	55.07
x=0.5	0.85	0.71	65.24

The hysteresis factor is an important factor that represents the reversibility of hydrogen absorption and desorption of the hydrogen storage alloys. It is clearly observed from Table 3 that H_f decreases from 1.06 (x=0) to 0.71 (x=0.5) with increase of Sn content in the alloys. On the other hand, the reversibility between hydrogen absorption and desorption is improved by increase of Sn content in the alloys and eventually results in the decrease of H_f. This suggests that increase of $LaNi_5$ cell volume may enhance the hydrogen storage capability. As indicated by HUANG et al [14], the increase of crystal cell volume reduces the pressure of hydrogen absorption and desorption of the alloys.

The slope factor can explain the plateau performance of hydrogen absorption. It is seen from Table 3 that S_f is enhanced from 38.85% (x=0) to 65.24% (x=0.5) with increase of Sn content in the alloys, which means that plateau performance of hydrogen absorption is weakened. HUANG et al [14] and ZHOU et al [15] showed that H_f and S_f are strongly influenced by homogenous composition. The homogenous composition and perfected structure improve the plateau performance of hydrogen absorption. It may be assumed that homogeneity of phases of the alloys decreases with increasing Sn content.

3.3 Electrochemical discharge characteristics

Figure 4 shows the activation profiles of the $La_{0.7}Mg_{0.3}Al_{0.3}Mn_{0.4}Co_{0.5-x}Sn_xNi_{3.8}$ (x=0−0.5) alloys electrodes. It can be seen that all electrodes can be easily activated to their maximum discharge capacity within five cycles.

The maximum discharge capacities (C_{max}) of the electrode alloys are summarized in Table 4. It can be seen clearly that electrochemical capacity decreases markedly from 337.1 mA·h/g (x=0) to 239.8 mA·h/g (x=0.5) with the increase in Sn content. However, a close

inspection reveals that with small Sn content, such as $La_{0.7}Mg_{0.3}Al_{0.3}Mn_{0.4}Co_{0.4}Sn_{0.1}Ni_{3.8}$ (x=0.1), the maximum discharge capacity only decreases by 1.5% and the capacity retention increases by 1.1% compared with Sn-free alloy (x=0). These results are similar to $MlNi_{(4.45-x)}Mn_{0.4}Al_{0.15}Sn_x$ reported by MA et al [16]. The discharge capacity of the $MlNi_{(4.45-x)}Mn_{0.4}Al_{0.15}Sn_x$ electrode alloys decreases from 343.2 mA·h/g (x=0) to 235.4 mA·h/g (x=0.5) with increase of Sn content.

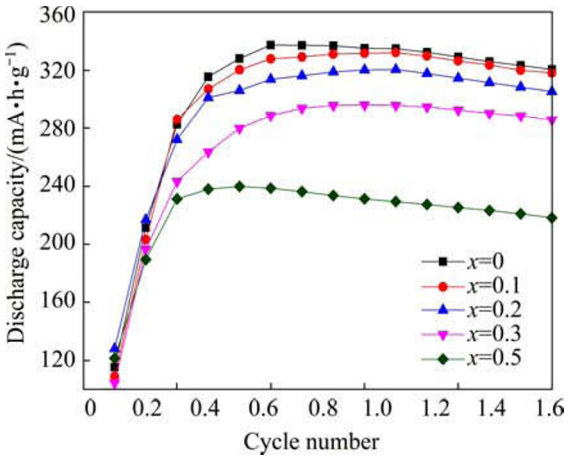

Fig. 4 Activation profiles of $La_{0.7}Mg_{0.3}Al_{0.3}Mn_{0.4}Co_{0.5-x}Sn_xNi_{3.8}$ (x=0−0.5) alloys

Table 4 Electrochemical properties of $La_{0.7}Mg_{0.3}Al_{0.3}Mn_{0.4}Co_{0.5-x}Sn_xNi_{3.8}$ (x=0−0.5) alloys

Sample	C_{max}/(mA·h·g^{-1})	(C_{100}/C_{max})/%	HRD_{1400}/%*
x=0	337.1	70.2	68.4
x=0.1	332.1	71.3	50.4
x=0.2	320.5	72.1	36.2
x=0.3	296.1	77.2	27.2
x=0.5	239.8	78.0	25.7

* The high rate dischargeability at a current density of 1400 mA/g

As indicated by MUNGOLE et al [17], the decrease in the discharge capacity can be ascribed to the formation of the precipitate phase. In our case, we found that the formation and increase of the LaNiSn phase in AB_5 type hydrogen storage alloys resulted in the decrease of hydrogen storage capacity and also electrochemical discharge capacity as shown in Fig. 5, indicating the correlation between the maximum hydrogen storage and electrochemical discharge capacity of the $La_{0.7}Mg_{0.3}Al_{0.3}Mn_{0.4}Co_{0.5-x}Sn_xNi_{3.8}$ (x=0−0.5) alloys.

Figure 6 shows the cycle life curves of the alloy electrodes. The discharge capacity retentions of the alloy electrodes after 100 charge−discharge cycles, C_{100}/C_{max}, are also listed in Table 4, where C_{100} is the discharge capacity of the 100th cycle. It can be seen from Table 4 that the discharge capacity retentions of the electrodes increase from 70.2% (x=0) to 78.0% (x=0.5) after 100

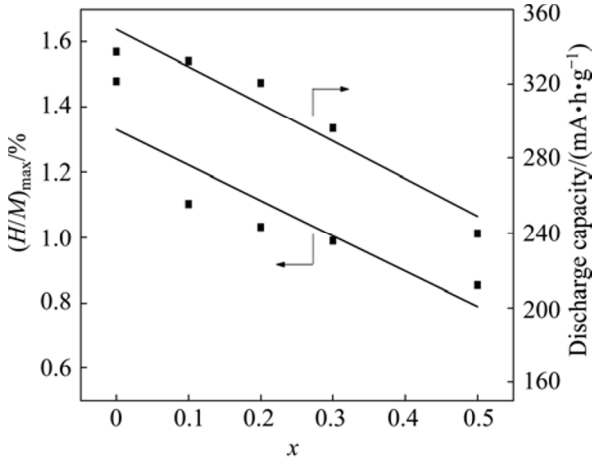

Fig. 5 Hydrogen storage and electrochemical discharge capacity of $La_{0.7}Mg_{0.3}Al_{0.3}Mn_{0.4}Co_{0.5-x}Sn_xNi_{3.8}$ (x=0−0.5) alloys

charge−discharge cycles. The pulverization of the alloy particles during the electrochemical tests may be the main reason of efficacy loss of hydrogen storage capacity of the alloy electrode. The oxidation and corrosion layer increased resistance to hydrogen adsorption and desorption during the pulverization of the alloy in alkaline electrolyte. We also considered that the consequences of oxidation and corrosion layers created a barrier of diffusion of hydrogen atoms in the alloy electrode and decreased drastically property of hydrogen absorption and desorption during the charge−discharge cycling. Therefore, it can be concluded that with the increase of Sn content in the alloy, the corrosion and pulverization resistance of the alloys increases. As put forward by LIN et al [18], the evidence of increasing the cycle life was explained by formation of a passive SnO_2 layer on the surface of the alloy particles, preventing the pulverization of electrode materials during the cycling.

Figure 7 shows the high-rate dischargeability (HRD) of the $La_{0.7}Mg_{0.3}Al_{0.3}Mn_{0.4}Co_{0.5-x}Sn_xNi_{3.8}$ (x=0−0.5) hydrogen storage alloy electrodes. The HRD, a main

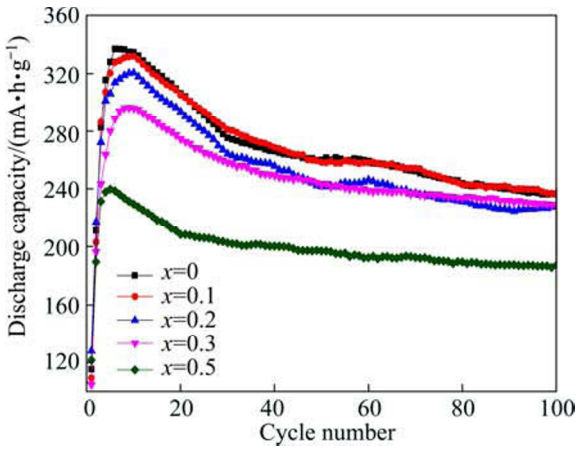

Fig. 6 Cyclic stability of $La_{0.7}Mg_{0.3}Al_{0.3}Mn_{0.4}Co_{0.5-x}Sn_xNi_{3.8}$ (x=0−0.5) alloys

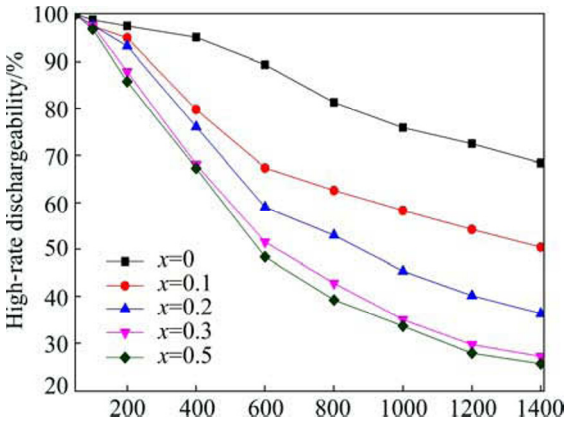

Fig. 7 High-rate dischargeability of $La_{0.7}Mg_{0.3}Al_{0.3}Mn_{0.4}Co_{0.5-x}Sn_xNi_{3.8}$ (x=0−0.5) alloys

factor that represents the kinetic property of hydrogen storage alloy electrode, is calculated according to the following formula:

$$\mathrm{HRD}=\frac{C_{\mathrm{d}}}{C_{\mathrm{d}}+C_{50}}\times 100\% \quad (2)$$

where C_d is a discharge capacity with a cut-off potential of 0.8 V at the discharge current density J_d; C_{50} is the residual discharge capacity with a cut-off potential of 0.8 V at the discharge current density J= 50 mA/g also after the electrode has been fully discharged at J_d. The HRD at 1400 mA/g is also listed in Table 4. It is apparent from Fig. 7 that HRD decreased when Sn content increased in the alloys. Taking the discharge current density J_d=1000 mA/g as an example, the HRD decreased drastically from 72.5% (x=0) to 27.9% (x=0.5). These values have similarities for $Ml_{(4.45-x)}Mn_{0.4}Al_{0.15}Sn_x$ studied by MA et al [16], who reported that the HRD decreased by almost five times when Sn content increased in alloys. It is believed that the decrease of HRD caused by Sn substitution may be attributed to a formation of SnO_2 as reported by LIN et al [18]. The further research would be to study the influence of Sn content on corrosion resistance of the alloys.

4 Conclusions

This paper investigated the influence of substitution of cobalt by tin on the microstructure, hydrogen storage performance and electrochemical properties of the $La_{0.7}Mg_{0.3}Al_{0.3}Mn_{0.4}Co_{0.5-x}Sn_xNi_{3.8}$ (x=0−0.5) hydrogen storage alloys. The increasing substitution of Sn for Co resulted in the increase of LaNiSn phase content and cell volume of $LaNi_5$ phase, and the decrease of $LaNi_5$ phase content. The hydrogen storage capacity and hysteresis factor of the hydrogen absorption and desorption decreased with enhancement of sloping factor when increasing the substitution amount of Sn for Co. When the substituted amount of Sn for Co increased from x=0 to x=0.5, the electrochemical measurements showed that the maximum discharge capacity decreased from 337.1 mA·h/g to 239.8 mA·h/g; the discharge capacity retention at the 100th cycle increased from 70.2% to 78.0%; at a discharge current density of 1400 mA/g, the high-rate dischargeability of the alloy electrodes decreased from 68.4% to 25.7%.

Acknowledgements

The authors wish to thank Institute for Superconducting and Electronic Materials (ISEM), University of Wollongong and Institute Nuclear and Energy Research (IPEN), University of São Paulo for the financial support and thanks are also given to National Council for Scientific and Technological Development – CNPQ – Brazil for the scholarships and financial support (CNPQ 472504/2010-0) granted to Julio Cesar Serafim CASINI.

References

[1] FENG F, GENG M, NORTHWOOD D O. Electrochemical behaviour of intermetallic-based metal hydrides used in Ni/metal hydride (MH) batteries: A review [J]. Int J Hydrogen Energy, 2001, 26: 725−734.

[2] LIU Y, PAN H, GAO M, LI R, LEI Y. Effect of Co content on the structural and electrochemial properties of the $La_{0.7}Mg_{0.3}Ni_{3.4-x}Mn_{0.1}Co_x$ hydride alloys I: The structure and hydrogen storage [J]. J Alloys Compd, 2004, 376: 296−303.

[3] LIU Y, PAN H, GAO M, LI R, LEI Y. Effect of Co content on the structural and electrochemial properties of the $La_{0.7}Mg_{0.3}Ni_{3.4-x}Mn_{0.1}Co_x$ hydride alloys II: Electrochemical properties [J]. J Alloys Compd, 2004, 376: 304−313.

[4] ZHANG P, WEI X, LIU Y, ZHU J, ZHANG Z, ZHAO T. The microstructure and electrochemical properties of non-stoichiometric low-Co AB_5 alloys containing small amounts of Mg [J]. J Alloys Compd, 2005, 399: 270−275.

[5] CUSCUETA D, MELNICHUCK M, PERETTI H A, SALVA H R, GHILARDUCCI A A. Magnesium influence in the electrochemical properties of La−Ni base alloy for Ni−MH batteries [J]. Int J Hydrogen Energy, 2008, 33: 3566−3570.

[6] FERREIRA E A, SERRA J M, CASINI J C, TAKIISHI H, FARIA R N. Microstructure and electrochemical properties of a LaMgAlMnCoNi based alloy for Ni/MH batteries [J]. Materials Science Forum, 2012, 727−728: 80−84.

[7] BROWMAN R C, LUO C H, AHN C C, WITHAM C K, FULTZ B. The effect of tin on the degradation of $LaNi_{5-y}Sn_y$ metal hydrides during thermal cycling [J]. J Alloys Compd, 1995, 217: 185−192.

[8] LAMBERT S W, CHANDRA D, CATHEY W N, LYNCH F E, BOWMAN R C. Investigation of hydriding properties of $LaNi_{4.8}Sn_{0.2}$, $LaNi_{4.27}Sn_{0.24}$ and $La_{0.9}Gd_{0.1}Ni_5$ after thermal cycling and aging [J]. J Alloys Compd, 1992, 187: 113−135.

[9] VOGT T, REILLY J J, JOHNSON J R, ADZIC G D, MCBREEN J. Crystal structure of nonstoichiometric $La(Ni,Sn)_{5+x}$ alloys and their properties as metal hydride electrodes [J]. Electrochem Solid-State Letters, 1999, 2: 111−114.

[10] KUMAR M P, ZHANG W, PETROV K, ROSTAMI A, SRINIVASAN, ADZIC G D, JOHNSON J R, REILLY J J. Effect of Ce, Co, and Sn substitution on gas phase and electrochemical

hydriding/dehydriding properties of $LaNi_5$ [J]. Electrochem Soc, 1995, 142: 3424−3428.

[11] ZHANG P, LIU Y, ZHU J, WEI X, YU G. Effect of Al and W substitution for Ni on the microstructure and electrochemical properties of $La_{1.3}CaMg_{0.7}Ni_{9-x}(Al_{0.5}W_{0.5})_x$ hydrogen storage alloys [J]. Int J Hydrogen Energy, 2007, 32: 2488−2493.

[12] REN J, ZHANG Y, FENG M, WANG G, ZHAO X, WANG X. Microstructures and electrochemical properties of cobalt-free $LaNi_{4.0}Al_{0.2}Fe_{0.4}Cu_{0.4-x}Sn_x$ (x=0−0.4) electrode alloys prepared by casting [J]. J Rare Earths, 2006, 24: 574−578.

[13] LIU Y, PAN H, ZHU Y, LI R, LEI Y. Influence of Mn content on the structural and electrochemical properties of the $La_{0.7}Mg_{0.3}Ni_{4.25-x}Co_{0.75}Mn_x$ hydrogen storage alloys [J]. Materials Science and Engineering A, 2004, 372: 163−172.

[14] HUANG T, HAN J, ZHANG Y, YU J, SUN G, REN H, YUAN X. Study on the structure and hydrogen absorption-desorption characteristics of as-cast and annealed $La_{0.78}Mg_{0.22}Ni_{3.48}Co_{0.22}Cu_{0.12}$ alloys [J]. J Power Source, 2011, 196: 9585−9589.

[15] ZHOU Z, SONG Y, CUI S, HUANG C, QIAN W, LIN C, ZHANG Y, LIN Y. Effect of annealing treatment on structure and electrochemical performance of quenched $MmNi_{4.2}Co_{0.3}Mn_{0.4}Al_{0.3}Mg_{0.03}$ hydrogen storage alloy [J]. J Alloys Compd, 2010, 501: 47−53.

[16] MA J, PAN H, CHEN C, WANG Q. The electrochemical properties of Co-free AB_5 type $Ml_{(4.45-x)}Mn_{0.4}Al_{0.15}Sn_x$ hydride electrode alloys [J]. J Alloys Compd, 2002, 343: 164−169.

[17] MUNGOLE M N, BALASUBRAMANIAM R, RAI K N. Correlation between microstructure and hydrogen storage capacity in $MnNi_5$ alloys with Al, Mn and Sn substitutions [J]. Int J Hydrogen Energy, 1999, 24: 467−471.

[18] LIN Q, ZHAO S, ZHU D, SONG B, MEI Z. Investigation of hydriding properties and structure of $MlNi_{5-x}Sn_x$ system [J]. J Alloys Compd, 2003, 351: 91−94.

Sn 替换 Co 对 AB_5 型 $La_{0.7}Mg_{0.3}Al_{0.3}Mn_{0.4}Co_{0.5-x}Sn_xNi_{3.8}$ (x=0−0.5)合金显微结构和电化学性能的影响

Julio Cesar Serafim CASINI[1,2], Zai-ping GUO[1], Hua Kun LIU[1],
Eliner Affonso FERREIRA[2], Rubens Nunes FARIA[2], Hidetoshi TAKIISHI[2]

1. Institute for Semiconducting and Electronic Materials, University of Wollongong, NSW 2522, Australia;
2. Materials Science and Technology Center, Nuclear and Energy Research Institute,
University of São Paulo, SP 05508-900, Brazil

摘　要: 采用 X 射线衍射方法、压力−成分等温线、电化学放电循环研究了 AB_5 型 $La_{0.7}Mg_{0.3}Al_{0.3}Mn_{0.4}Co_{0.5-x}Sn_xNi_{3.8}$ (x=0, 0.1, 0.2, 0.3, 0.5)合金中用 Sn 替换 Co 对其显微结构、储氢性能和电化学放电容量的影响。XRD、SEM 及 EDS 测试结果表明，所有的合金都主要由 $LaNi_5$ 和 $MgNi_2$ 相组成，但随着合金中 Sn 含量的逐渐增加，出现 LaNiSn 相且显微结构得到细化。压力−成分等温线表明，随着合金中 Sn 含量的增加，合金的最大储氢容量从 1.48%(x=0)降低到 0.85%(x=0.5)。电化学测试结果表明，随着合金中 Sn 含量的增加，合金的最大放电容量从 337.1 mA·h/g(x=0)降低到 249.8 mA·h/g(x=0.5)；充放电循环 100 次的放电容量保持率从 70.2%(x=0)增加到 78.0%(x=0.5)。

关键词: 储氢合金；显微组织；镍氢电池；Sn; Co；取代

(Edited by Hua YANG)